

# Analytical and experimental fatigue analysis of wind turbine tower connection bolts

Behrouz Badrkhani Ajaei\* and Serdar Soyoz<sup>a</sup>

Department of Civil Engineering, Bogazici University, Istanbul, Turkey

(Received July 20, 2020, Revised April 30, 2020, Accepted May 28, 2020)

**Abstract.** This paper presents a method of estimation of fatigue demands on connection bolts of tubular steel wind turbine towers. The presented method relies on numerical simulation of aerodynamic loads and structural behavior of bolted connections modeled using finite element method. Variability of wind parameters is represented by a set of values derived from their probability densities, which are adjusted based on field measurements. Numerically generated stress time-series show agreement with the measurements from strain gauges inside bolts, in terms of power spectra and the resulting damage. Position of each bolt has a determining effect on its fatigue damage. The proposed framework for fatigue life estimation represents the complexities in loading and local behavior of the structure. On the other hand, the developed procedure is computationally efficient since it requires a limited number of simulations for statistically representing the wind variations.

**Keywords:** wind turbine; tower; fatigue; finite element; aero-dynamic; bolted connection

## 1. Introduction

Due to the cyclic nature of the loads sustained by wind turbine towers, fatigue is a major contributor to structural failures in these towers. Although many other types of structures including bridges are also under the risk of fatigue damage as a result of persistent vibration due to wind loads (Mao and Zhou 2017), wind turbine towers are under the influence of multiple sources of load fluctuations, including periodic aerodynamic forces caused by wind shear, effect of wind turbulence, and dynamic effects of mechanical parts (Ilhan *et al.* 2018). Consequently, fatigue is one of the major subjects covered in wind turbine design and certification codes including GL (2010), and IEC (2005). SHK (2017) indicated occurrence of fatigue in bolts as the reason for the tower collapse in Lemnhult. Chou and Tu (2011) also report some cases of fatigue damage in wind turbines. In addition to financial losses that may arise from structural failure of wind turbines, human safety is also a concern (Robinson *et al.* 2013).

Various types of connections have been used in wind turbine towers (Heistermann *et al.* 2009, Pavlović *et al.* 2015). This paper focuses on the bolted flange connections, which is a very popular connection type commonly used for tubular wind turbine towers all over the world.

A review of the existing literature in the subject of fatigue in wind turbine towers and the general subject of fatigue reveals that different research projects that are conducted in this subject have adopted different approaches.

The approaches and methodologies adopted by researchers can be broadly put into the following three categories: Laboratory Experiments, In-field measurements or health monitoring, and Analytical or numerical studies. However, there may be some research projects that do not fall into these categories, or they may be combinations of two or more of these approaches (e.g., Seidel and Schaumann 2001).

Different components of a wind turbine including rotor blades, tower, and mechanical parts may experience fatigue damage. Hamdi and Farah (2018) indicate that sustained vibration of the rotor blades can lead to damage in the blades. Shirani and Härkegård (2011a, 2011b) investigated fatigue in cast iron material used in wind turbine components. However, fatigue as a type of structural damage is highly sensitive to material and type of loading. While fatigue failure of mechanical components of the turbine results in inability of the turbine to produce power, failure of the connections of the tower may result in collapse and total destruction of the turbine. Due to very large dimensions of wind turbine towers and their connections, full-scale fatigue and fracture experiments on these structures are not practical. Experimental studies in this subject are usually focused on fatigue strength of bolts or small parts of the connection region (e.g., Schaumann and Eichstädt 2015, Oechsner *et al.* 2015). One major drawback of these types of experiments is that the loading applied to small parts of the connection in the laboratory may not reflect the complex effects of the aerodynamic loads of the turbine on the bolted connection. Van-Long *et al.* (2013) conducted tests on bolted flange plate connections, used in circular tubular structures which are much smaller than connections used in wind turbines, and are subjected to a different type of loading.

In-field measurements and health monitoring is another approach commonly taken by the researchers of this field.

---

\*Corresponding author, Ph.D. Candidate

E-mail: behrouz.ajaei@boun.edu.tr

<sup>a</sup>Associate Professor

E-mail: serdar.soyoz@boun.edu.tr

Pollino and Huckelbridge (2012) obtained stress time histories throughout a year, by in-situ measurements from strain gauges installed on a wind turbine tower. Relying on strain measurements for fatigue life estimation may be insufficient due to the possibility of missing out special conditions that are statistically likely in the lifetime of the structure, but have not occurred during the measurement period. Benedetti *et al.* (2013), suggests a health monitoring scheme of detecting fatigue cracks in bases of the walls of wind turbine towers, by placing numerous strain sensors around the circumference of the tower wall, with small distances between them shorter than the crack length to be detected. The health monitoring approach, though is very useful in understanding the real behavior of the structure, cannot substitute numerical simulation since it requires installing a large number of strain gauges in all the critical points of the structure.

Analytical and numerical methods in addition to being economically more affordable are also very flexible in their capability to take as input many different sets of wind conditions. Therefore, numerical simulation is a necessary part of fatigue analysis of these structures.

Analytical and numerical studies have been previously conducted on damage in bolted connections in general. Blachowski and Gutkowski (2016) studied the effects of damaged bolted connections on behavior of a telecommunication tower. However, wind turbines have unique aerodynamic behavior that make them different from other structures, and distinguishes this subject from the subject of fatigue in other types of structures.

Numerical procedures commonly used for fatigue design or evaluation of wind turbine towers usually take simplified approaches regarding the local behavior of the critical regions and components where fatigue damage is likely to occur. Do *et al.* (2014a, 2014b) assumed the fatigue damage occurring in the tower wall at the base of tower. Commonly a linear relationship is assumed between force (or bending moment) and stress (e.g., Annex G of IEC, 2005) and cycle-counting is done on force (or bending moment) instead of stress. However, for behavior of complex assemblies like behavior of preloaded bolts in ring-shaped flange connections (which is in the scope of this paper) these types of assumptions are not correct, as it is well-known that in the case of preloaded bolts, only a small portion of changes in external load ranges is transferred to the bolts (Williams *et al.* 2009, Pedersen and Pedersen 2008a, 2008b).

In order to have accurate estimations of fatigue damage and fatigue life of wind turbine towers, it is essential to have analytical and numerical methods of fatigue analysis that include different aspects of the problem, including aerodynamic-structural interactions of the tower and blades, changes in rotational speed of the rotor, local effects of the geometry and structural details of the connections, and variations of wind speed and turbulence.

This paper presents a numerical method of estimating fatigue demands on connection bolts of bolted flange type connections of tubular steel wind turbine towers. The main objective of this research is to present a numerical procedure of fatigue life estimation that takes into

consideration the variability of wind and complexities of aero-dynamic loads and bolted connections while it is applicable in the industry. A procedure is developed to take into account the variability of wind speed parameters by sets of wind parameters chosen based on probability distributions of those parameters. Wind load effects on the structure are calculated by coupled aero-dynamic analyses using the FAST (Jonkman and Buhl 2005) software. Internal forces and displacements of the tower calculated by aero-dynamic analyses are applied to the boundaries of a finite element model of the bolted connection produced in the ABAQUS (1998) software. Walls and flanges of the connection are modeled by shell elements, and bolts are modeled by beam elements in which preloads are applied by fictitious thermal deformations. Stresses experienced by the bolts are calculated by the finite element analyses. Results of the finite element analyses show consistency with strain records from strain gauges inside the bolts. The rainflow cycle-counting procedure of ASTM (1997) is applied to the calculated stress time-series, and stress range histograms are obtained, which are combined based on the probabilities assigned to different sets of wind parameters. The S-N curve suggested by Eurocode (2005b) are modified considering the type of the structure and probability of survival, and is used along with the stress range histograms and the Miner's damage index, in order to estimate the average accumulated fatigue damages in a certain time period. Based on the average accumulated fatigue damages, fatigue lives of the bolts are estimated.

This paper presents an integrated numerical-experimental framework for fatigue analysis of wind turbine tower connection bolts. Results of this research do not determine the quality or safety of products of any specific manufacturer or designer.

## 2. The Case study wind turbine tower

The case study wind turbine for this research is installed in Saritepe Campus of Bogazici University and is shown in Fig. 1. It is a 900 kW variable speed on-shore turbine, has a three-bladed upwind rotor, has a rotor diameter of 44 m, and a hub height of 55 m.

The steel tower is made of three parts which are shown with different colors in the schematic drawing of Fig. 2. The three parts of the steel tower are connected to each other by bolted circular flange connections. The connection connecting the lower and middle parts of the tower is marked in Fig. 2, and its top view is shown in Fig. 3. There are 88 M36 (grade 10.9) bolts in that connection, with a design preload of 510 kN. Fig. 4 shows the view from the Section A-A of the connection. In this paper, the positions of the bolts around the circular flange connection are referred to by their clockwise angular positions with respect to North, as shown in Fig. 3. Bolts positioned at 233° and 110° positions are instrumented with strain gauges in their shanks.

A weather station shown in Fig. 5 is positioned at a 204 m distance from the tower, in the South-West direction. An ultrasonic device is installed at a height of 60 m from



Fig. 1 A picture of the wind turbine at Bogazici University

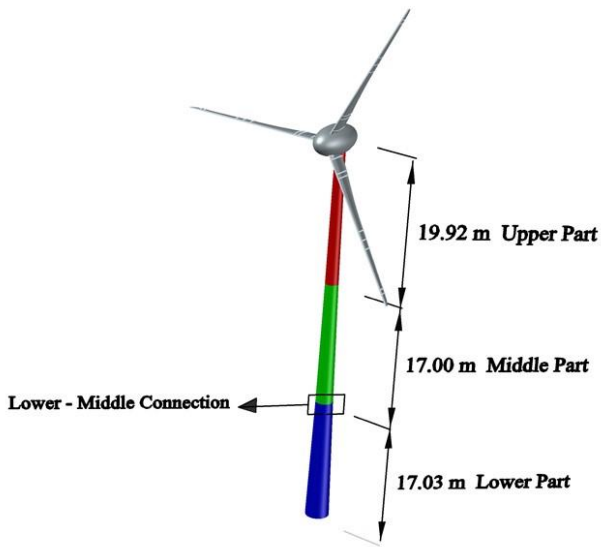


Fig. 2 Three parts of the steel tower

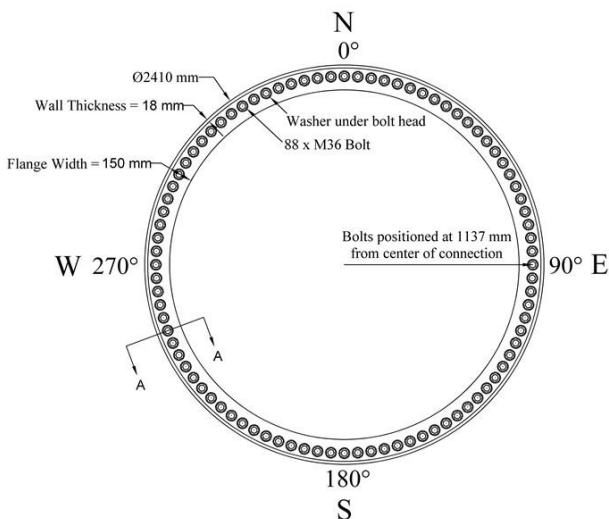


Fig. 3 Top view of the Lower - Middle connection

ground, which measures short-term average wind speed ( $V_a$ ), standard deviation of wind speed ( $\sigma_V$ ), and wind direction angle ( $\theta$ ) with respect to North.

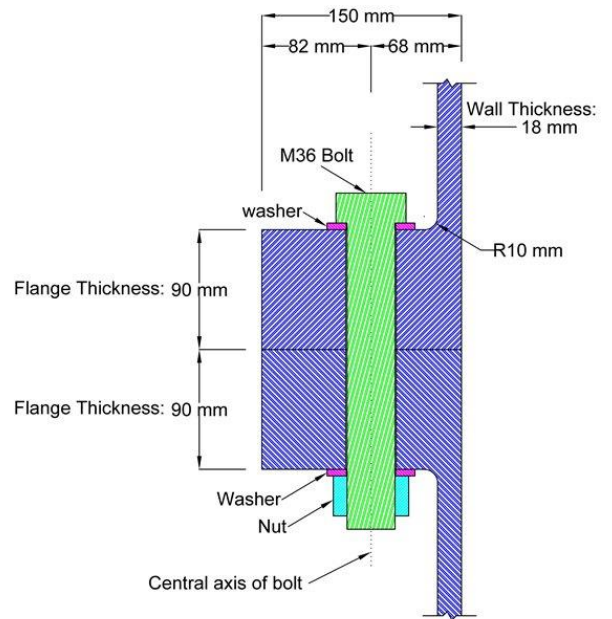


Fig. 4 View from the Section A-A of the bolted connection



Fig. 5 The weather station near the wind turbine

### 3. Simulation of the aero-dynamic loads

Different approaches can be taken to estimate the aerodynamic loads on many types of structures under wind loading, including wind measurements on full-scale structures, small-scale experiments, wind tunnel tests, and numerical simulations (Lu *et al.* 2016, Gol-Zaroudi and Aly 2017, Elshaer *et al.* 2019). In this research, aerodynamic loads on the turbine and the tower are calculated by numerical simulation. As a result of continuous research on wind turbine modeling, methods of numerical analysis of wind turbine towers have evolved from simplified single degree of freedom models to more accurate methods that employ aerodynamic models together with finite element models (Ke *et al.* 2016). In this research, the FAST software (Jonkman and Buhl, 2005) is used for aerodynamic analyses, which uses the Blade Element Momentum Method for calculating the aerodynamic loads.

Mean wind speed and turbulence intensity are two parameters commonly measured by weather stations and used for characterizing the wind flow in an event or a specific site

(Gunter *et al.* 2017). In this research, the measurements of these two parameters by the weather station near the wind turbine are used to adjust the parameters of the numerically generated wind speed time-series.

The fatigue analysis performed in this research takes into account the fatigue damage accumulated in the operational conditions, shot-down, and start-up events. Consequently, the aero-dynamic loads applied to the structure in these conditions need to be simulated.

### 3.1 Variations of Wind Parameters

In order to conduct aerodynamic analyses, time series of wind speed are needed. Two major parameters of wind speed time series that affect the fatigue damage are the wind speed average over the time series ( $V_a$ ), and Turbulence Intensity ( $TI$ ), defined by Eq. (1):

$$TI = \frac{\sigma_V}{V_a} \quad (1)$$

where  $\sigma_V$  is the standard deviation of wind speed ( $V$ ). In this research, Probability Density Functions (PDFs) of these wind parameters are used to choose the values of the wind parameters for which aerodynamic analyses are done. The design guidelines of IEC (2005) specify the types of PDFs for the parameters  $V_a$  and  $\sigma_V$ , and also provide empirical relationships for the parameters of those PDFs. The relationships given by IEC (2005) for estimation of the parameters of PDFs of  $V_a$  and  $\sigma_V$  aim to represent a wide range of possible wind turbine sites categorized into a few general categories, which may lead to overly conservative or unsafe estimates for the specific site at which the case-study wind turbine of this research is installed. Therefore, in this study the parameters of the mentioned PDFs are determined using wind measurements recorded by the weather station near the wind turbine.

Based on instructions of IEC (2005), a Rayleigh distribution with the Probability Density Function (PDF) as given in Eq. (2) can be assumed for variations of wind speed over an extended period of time.

$$\phi_{V_a}(V_a) = \frac{\pi V_a}{2V_{ave}^2} \exp\left[-\pi\left(\frac{V_a}{2V_{ave}}\right)^2\right] \quad (2)$$

where,  $V_a$  and  $V_{ave}$  denote the short term and long term averages of wind speed respectively.

A set of wind speed measurements are recorded by the weather station between 2015/04/01, 0:00 and 2015/04/02, 23:50. Based on the measurement sample of  $V_a$ , and the method explained in Appendix A, the parameter  $V_{ave}$  is estimated with the value  $\hat{V}_{ave} = 6.86\text{m/s}$ .

Fig. 6 shows the PDF of  $V_a$  with the parameter  $V_{ave}$  estimated as explained above, where the values that the variable  $V_a$  can take in the operational conditions (between the cut-in and cut-out wind speeds) are divided into six intervals separated by boundaries which are shown by

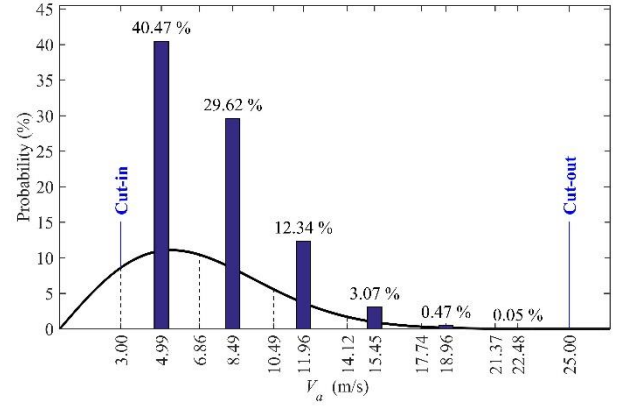


Fig. 6 PDF and Representative Values of  $V_a$

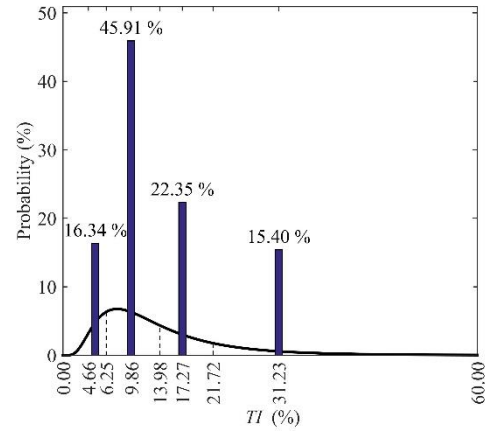


Fig. 7 PDF and Representative Values of  $TI$  for  $V_a = 4.99$  m/s

dashed vertical lines. In order to represent the variations of wind parameters by a limited number of generated wind speed time series, each one of the  $V_a$  intervals in Fig. 6 need to be represented by a single representative value of  $V_a$ . To calculate the representative value of each interval, a weighted average of  $V_a$  over each interval is calculated with the probability density ( $\phi_{V_a}$  according to Eq. (2)) used as the weighting factor. Probability of the  $V_a$  parameter being inside each interval is calculated by the area under the PDF curve in that interval, and is assigned to the representative value representing that interval. The representative values of  $V_a$  and the probabilities assigned to them are shown in Fig. 6 by a bar diagram.

Standard deviation of the wind speed at hub height over short periods of time (denoted by  $\sigma_V$ ) is a random variable in the life time of the turbine. IEC (2005) suggests a conditional log-normal probability distribution for  $\sigma_V$ , with mean value and standard deviation as given by Eqs. (3) and (4).

$$\mu_{\sigma_V|V_a} = I_{ref} (0.75V_a + 3.8\text{m/s}) \quad (3)$$

$$\sigma_{\sigma_V|V_a} = I_{ref} (1.4\text{m/s}) \quad (4)$$

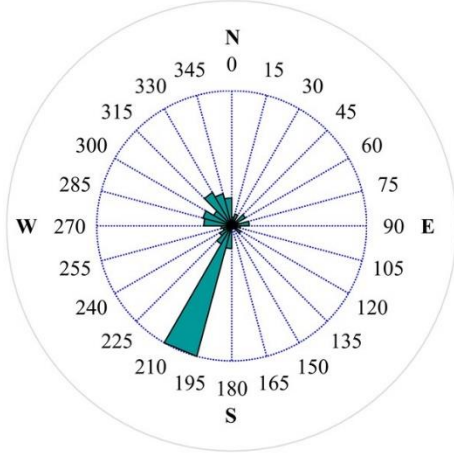


Fig. 8 Wind rose obtained from measurements

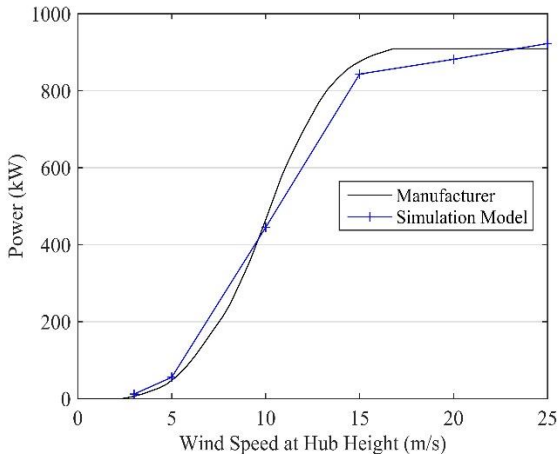


Fig. 9 Power curve obtained by the model vs. power curve of the case study turbine

where  $I_{ref}$  is the reference turbulence intensity, assumed to have a value of 0.16 for the class of the case study wind turbine. However, as illustrated in Appendix B, Eqs. (3) - (4) are not in agreement with the wind measurements recorded by the weather station. Based on the wind measurements and the procedure explained in Appendix B, Eqs. (5) - (6) are obtained for mean and standard deviation of  $TI$  for any specific value of  $V_a$ :

$$\mu_{TI|V_a} = \frac{0.1254V_a + 0.0721}{V_a} \quad (5)$$

$$\sigma_{TI|V_a} = \frac{0.48}{V_a} \quad (6)$$

Using Eqs. (5) and (6), the parameters of log-normal probability density functions of  $TI$  for each representative value of  $V_a$  can be calculated. Fig. 7 shows the PDF of  $TI$  for one of those representative values ( $V_a = 4.99\text{m/s}$ ). The values that the variable  $TI$  can take are divided into four intervals, and each interval is represented by a representative value, similar to the approach taken for the

$V_a$  parameter. The bar diagram showing the representative values of  $TI$  and the probabilities assigned to them is also shown in Fig. 7.

Similarly, for other representative values of  $V_a$ , the representative values for  $TI$  are obtained with their probabilities of occurrence. For each one of the six representative values of  $V_a$ , four representative values of  $TI$  are obtained, and consequently, 24 pairs of ( $V_a$ ,  $TI$ ) parameters are chosen as wind cases for the aerodynamic analyses.

The measurement records used for adjusting the wind speed parameters, also include the wind direction measurements. The wind rose shown in Fig. 8 is plotted based on the measurements of the ultrasonic device of the weather station. The wind rose shows a prevalent wind direction of  $202.5^\circ$  from North (Clockwise). Therefore, the rotor disc (together with nacelle) of the wind turbine model is aligned with the prevalent wind direction in the aerodynamic analyses. In the fatigue analyses of this research, the wind direction is assumed to be fixed in the prevalent wind direction. This is a safe approach if the fatigue damage conditions of the most critical bolts are taken as the basis for design and evaluation purposes, and the decisions are applied to all of the bolts equally.

### 3.2 Calculation of the aero-dynamic loads

In this research, the software TurbSim (Jonkman and Klicher 2012) is used to produce time-series of turbulent wind speed. For each set of representative  $V_a$  and  $TI$  values a wind field time-series is produced. The fields of wind speeds produced by the software TurbSim are used as inputs for aerodynamic analyses of the tower and rotor blades, using the software FAST (Jonkman and Buhl, 2005). The FAST software assumes fixed boundary conditions for the base of the tower. However, due to the soil and foundation flexibility the natural frequencies of a model with rigid base would be higher than the actual natural frequencies of the structure. Hanbay (2019) had performed operational modal analysis on 310 days of vibration measurements of the tower studied in this paper. The natural frequencies of the aero-dynamic model used in this paper are adjusted according to the results of the study by Hanbay (2019), by adding an extended length of 4.68 m to the base of the tower. Chord lengths of the rotor blades are taken from the values given by the turbine manufacturer. Other aerodynamic and control parameters (such as blade pitch controller and the airfoil shape) of the aerodynamic model are adjusted so that the rotational speed of the model does not exceed the range of rotational speed of the case study turbine (34.5 rpm), and also the power curve obtained by the model roughly fits the power curve of the case study turbine, as shown in Fig. 9.

Time-series of forces, bending moments and torque in a cross-section of the tower at a distance of 0.414 m above the bolted connection connecting the lower and middle parts of the tower are calculated by the FAST software. Also displacements and rotations in a cross-section 0.304 m below that connection are calculated. Fig. 10 shows time-series of the major bending moment at the cross-section

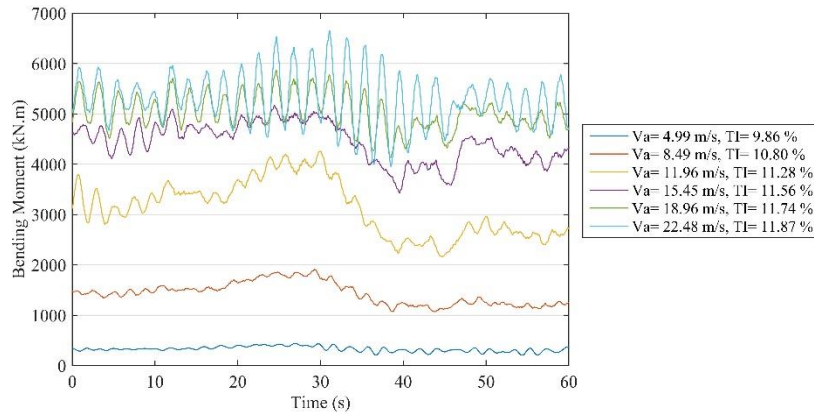


Fig. 10 Major bending moment above the connection calculated for different winds

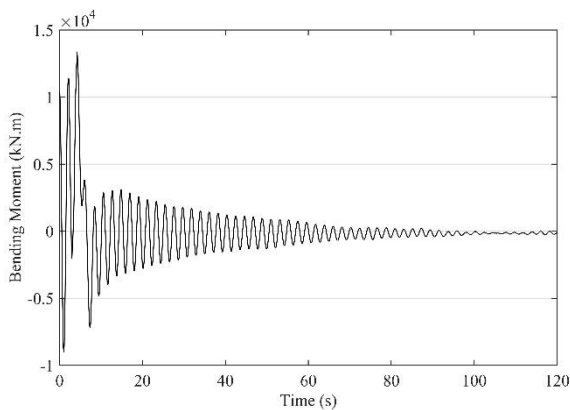


Fig. 11 Major bending moment in the shut-down event

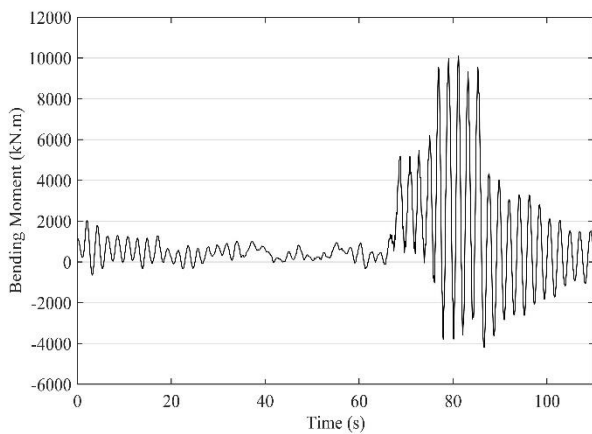


Fig. 12 Major bending moment in the start-up event

above the bolted connection for 6 of the total 24 wind cases (six different sets of  $V_a$  and  $TI$  values), with the turbine in the operating mode. The differences between the bending moment time-series at different wind speeds originate from several factors including the dependency of the aerodynamic forces on wind speed and the interferences of turbine control systems in higher wind speeds.

Figs. 11-12 show the time-series of the major bending moment above the connection, in shut-down and start-up events in the cut-out wind speed of 25 m/s and turbulence intensity of 12.83 %.

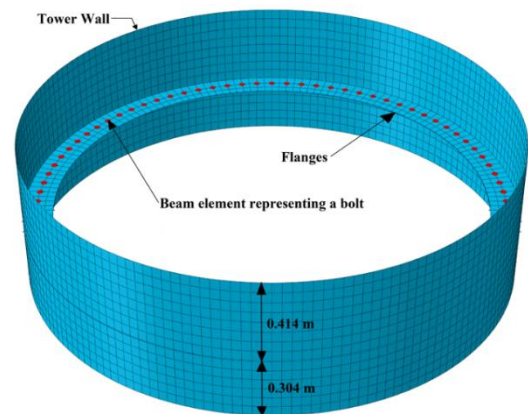


Fig. 13 Finite element model of the connection region

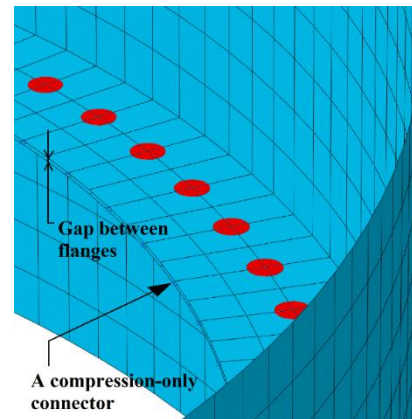


Fig. 14 A view of the finite element model around bolts and flanges

## 4. Finite element modeling of the connection region

### 4.1 Details of the model

A shell type finite element model of the bolted connection connecting the lower and middle parts of the tower (location of which is marked in Fig. 2 and details of it are shown in Figs. 3 and 4) is produced in ABAQUS (1998) finite element software. Flanges and wall of the tower connection are modeled by 3520 quadrilateral shell elements, while the 88 bolts connecting the two flanges are

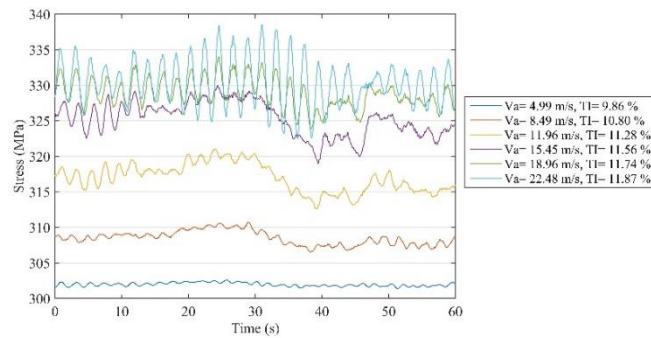


Fig. 15 Numerically generated stress time-series for the bolt at 233° position

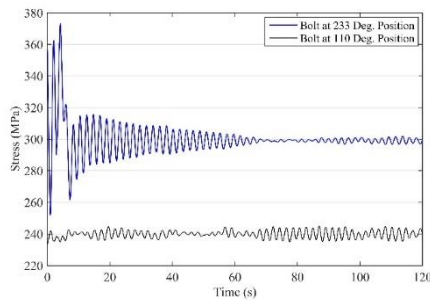


Fig. 16 Stress time-series of two bolts in shut-down event

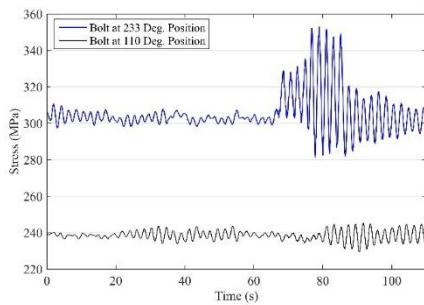


Fig. 17 Stress time-series of two bolts in start-up event

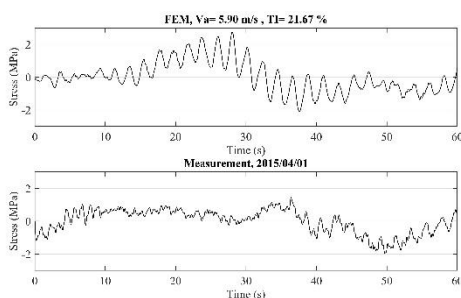


Fig. 18 Stress time-series from simulations and measurements of the bolt at 233° position

modeled by beam elements. Modulus of elasticity of steel is assumed to be  $E = 2.1 \times 10^5$  MPa and a Poisson's ratio of  $\nu = 0.3$  is assumed, according to Eurocode (2005a). Fig. 13 shows the finite element model developed for the connection. A 0.304 m segment of wall below the connection level and a 0.414 m segment above it are included in the model. In order to model the interaction

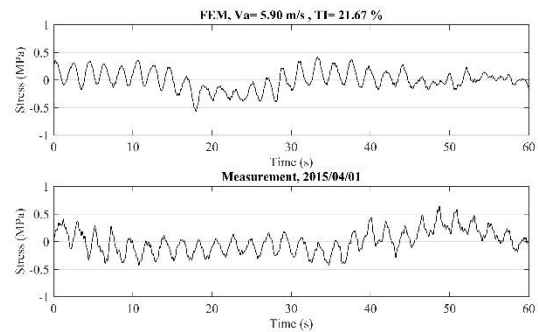


Fig. 19 Stress time-series from simulations and measurements of the bolt at 110° position

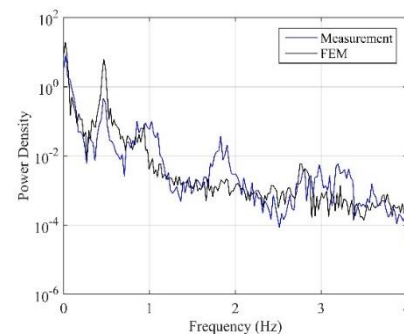


Fig. 20 Power spectral density of stress time-series, bolt at 233° position

between the flanges, a 4 mm gap is included between the shells representing the flanges as shown in Fig.14, and compression-only connector elements are placed between the nodes of the two flanges. Bolt preloads are applied by assigning coefficients of thermal expansion to the materials of beam elements and applying a fictitious temperature field to them. The forces and moments calculated by the aerodynamic analysis at the cross section above the connection and the displacements and rotations calculated at the cross section below the connection are applied as time-varying boundary conditions.

#### 4.2 Analysis results and strain records

Bolt stress time-series are then obtained from finite element analyses. Fig. 15 shows the stress time-series of the

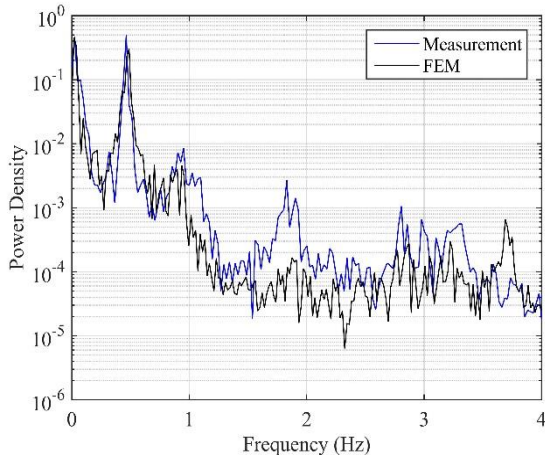


Fig. 21 Power spectral density of stress time-series, bolt at 110° position

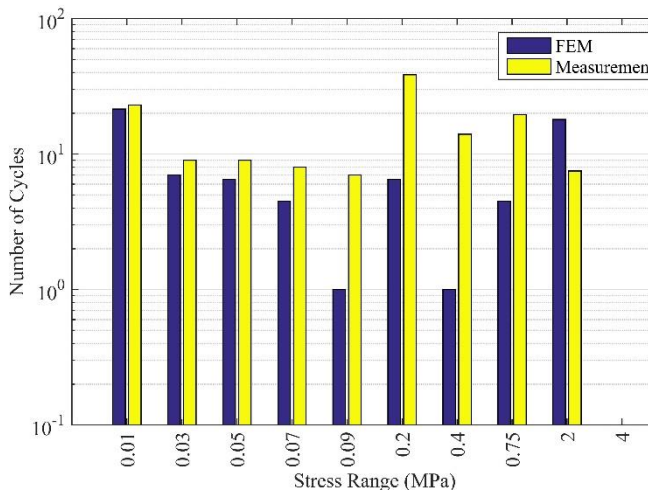


Fig. 22 Histograms of stress ranges in the bolt at 233° position, simulation vs. measurement

bolt in the 233° position, calculated for six sets of wind parameters, with the wind turbine in the operating conditions. Figs. 16 and 17 show the time-series of bolt stresses in shut-down and start-up events.

A strain record was obtained from strain gauges inside bolts at 233° and 110° positions on 2015/04/01, at 15:42:30. Wind speed measurements from the weather station, for that specific date and time, indicate an average wind speed of 5.90 m/s and a turbulence intensity of 21.67% for the hub height. Figs. 18 and 19 show the numerically generated stress time-series for bolts at 233° and 110° positions for wind parameters  $V_a = 5.90\text{m/s}$  and  $TI = 21.67\%$  and measurements from strain gauges inside those bolts recorded on 2015/04/01, at 15:42:30. Since fatigue damage is related to ranges of stress (or strain) cycles, the mean values are subtracted from strain records, and zero-mean stress time series are plotted.

Figs. 20 and 21 show the power density spectra of the stress time-series shown in Figs. 18 and 19. The plotted spectra show satisfactory agreement between the simulation and measurement results.

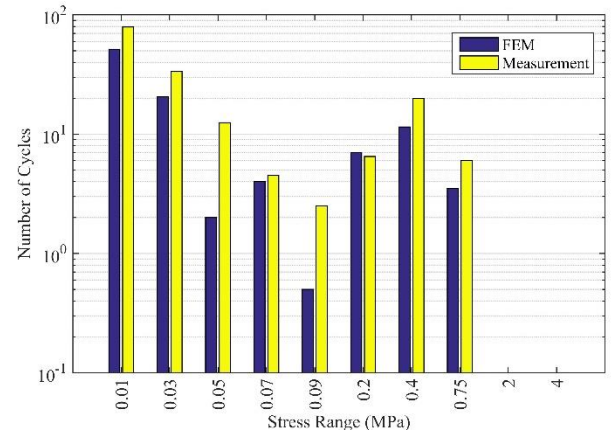


Fig. 23 Histograms of stress ranges in the bolt at 110° position, simulation vs. measurement

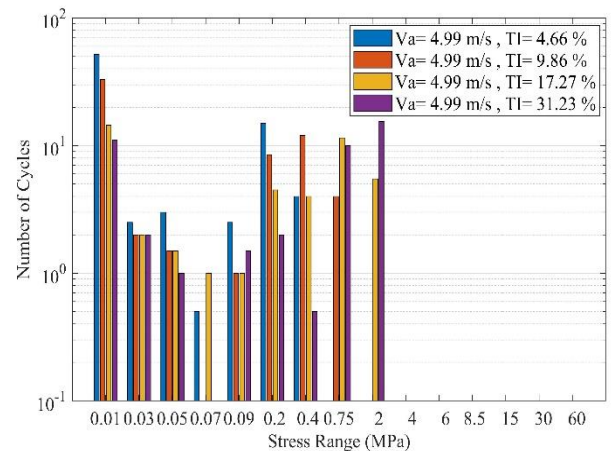


Fig. 24 Stress range histograms for Bolt at 233° position, for  $V_a = 4.99\text{ m/s}$  and different  $TI$  values in 1 min

## 5. Fatigue damage estimation procedure

In order to estimate the fatigue damage caused by an arbitrary stress time-series, first it should be converted to a set of constant amplitude cyclic time-series, with different stress ranges, using a procedure named cycle-counting. A computer program is developed to perform cycle-counting using the rainflow method according to the algorithm given in ASTM (1997). This method of cycle-counting is applied to all of the stress time-series obtained for sets of wind parameters.

Figs. 22 and 23 show the stress range histograms obtained by cycle counting the stress time-series shown in Figs. 18 and 19.

Fig. 24 shows the stress range histograms obtained by cycle counting the numerically generated stress time-series of the bolt at 233° position in 1 min of loading, calculated for the case of  $V_a = 4.99\text{m/s}$ , and different representative values of  $TI$ . In the same way, stress range histograms are obtained for all the other sets of representative values of wind parameters. Using the probabilities shown in Fig. 7 as weighting factors for the histograms shown in Fig. 24, the average stress range histogram for the case of

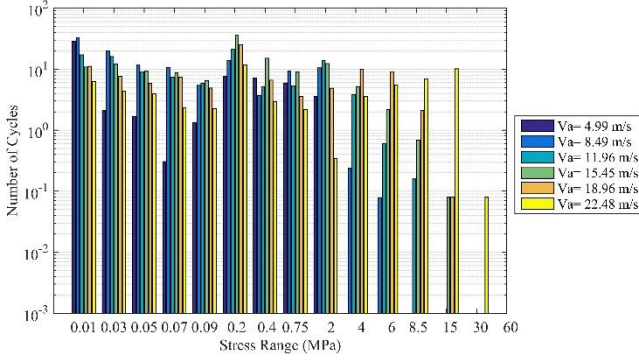


Fig. 25 Stress range histograms for Bolt at 233° position, for different  $V_a$  values in 1 min

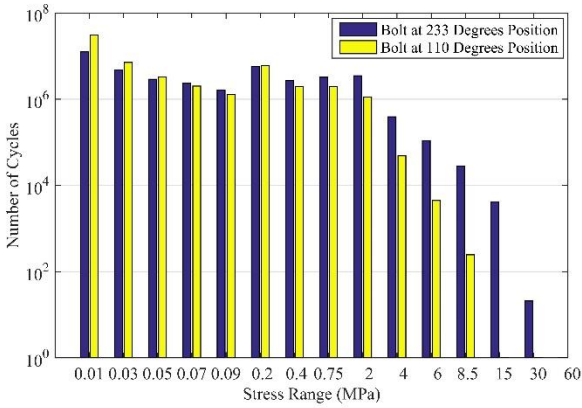


Fig. 26 Stress range histograms for two bolts in 1 year, caused by only operational times

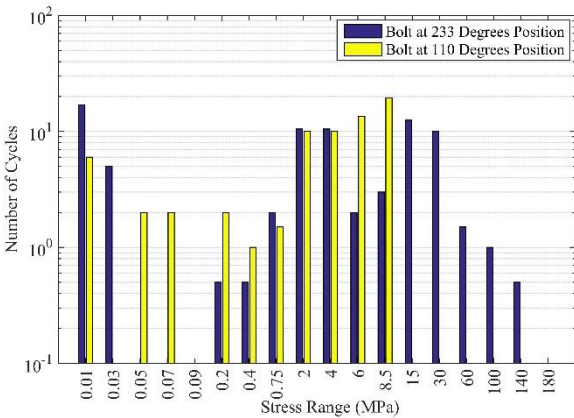


Fig. 27 Stress range histogram caused by a shut-down event

$V_a = 4.99\text{m/s}$  is calculated. Fig. 25 shows the stress range histograms of the bolt at 233° position for all the representative values of  $V_a$  obtained by applying the same procedure. The probabilities of occurrence shown in Fig. 6 are used as weighting factors for histograms shown in Fig. 25, and an average stress range histogram is obtained for the bolt at 233° position. Fig. 26 shows the average yearly stress range histograms obtained for the bolts at 233° and 110° position, caused only by operational times of the turbine. On the other hand, Figs. 27 and 28 show the stress range histograms caused by a shut-down and a start-up event.

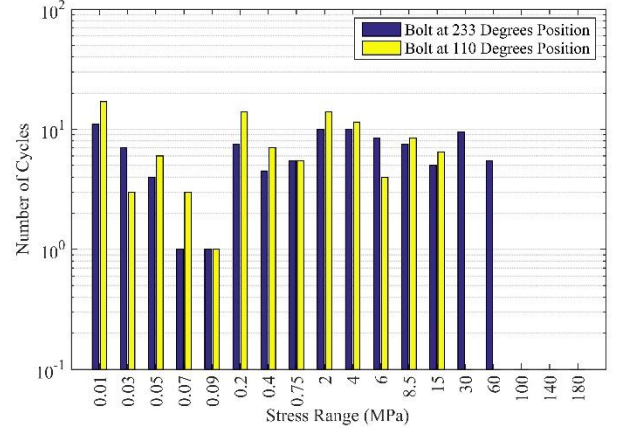


Fig. 28 Stress range histogram caused by a start-up event

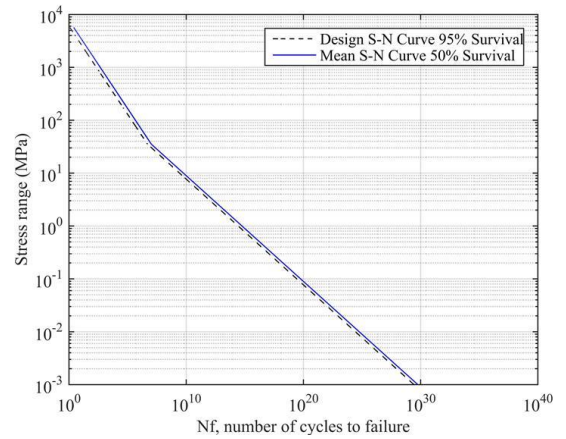


Fig. 29 The mean S-N curve obtained for M36 bolts

The Palmgren-Miner rule for damage summation as described in Eurocode (2005b) is used in this research. Miner's damage index can be calculated according to Eq. (7):

$$D = \sum_i \frac{n_i}{N_i} \quad (7)$$

where  $n_i$  is the number of stress cycles of a certain range, and  $N_i$  is the number of stress cycles with that range that would cause structural failure as a result of fatigue. It is assumed that when the damage index  $D$  reaches 1.0 failure due to fatigue occurs.  $N_i$  values for different stress ranges ( $S_i$ ) are usually provided in the form of S-N curves. The fatigue analyses of this research are based on the nominal stress method and employ the S-N curve provided by Eurocode (2005b) for the nominal stress method. The S-N curve that Eurocode (2005b) suggests for a bolt with a diameter larger than 30 mm (M36 bolts) corresponds to a 95 % survival probability for  $\text{Log}N$ , which is a conservative S-N curve suitable for design purposes. For evaluation purposes, a mean S-N curve (representing a 50 % survival probability) is needed. Therefore, assuming a normal distribution for  $\text{Log}N$ , the S-N curve of Eurocode (2005b) should be shifted as much as  $1.64 \times s_{\text{Log}N}$  towards higher values, where  $s_{\text{Log}N}$  is the standard deviation of  $\text{Log}N$  and is

Table 1 Damage accumulations from operational, shut-down, and start-up conditions

Bolt Position	Yearly Damage from operational times	Damage from a shut-down event	Damage from a start-up event
233°	$1.090 \times 10^{-5}$	$6.249 \times 10^{-6}$	$2.968 \times 10^{-6}$
110°	$2.281 \times 10^{-7}$	$1.704 \times 10^{-9}$	$9.305 \times 10^{-9}$

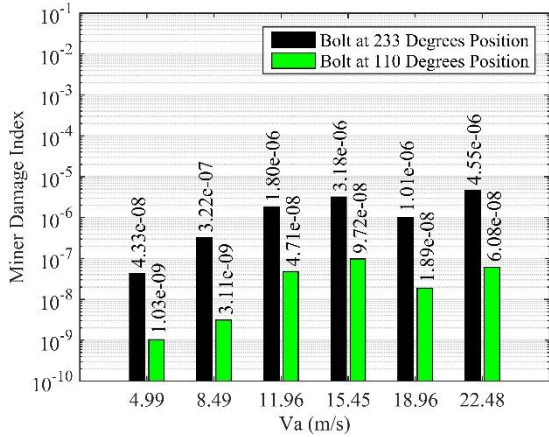


Fig. 30 Contribution of each wind speed to the yearly damage, in the operational conditions

assumed to be 0.2 for lack of information, as suggested by DNVGL (2016a). Moreover, the threshold value of fatigue strength (cut-off) is removed from the S-N curve, according to instruction of DNVGL (2016b). The mean S-N curve shown in Fig. 29 is used for damage calculations in this paper.

Using the stress range histograms of each bolt shown in Figs. 26, 27 and 28 and the mean S-N curve shown in Fig. 29, the yearly damage index accumulated in each bolt from operational times, and the damages accumulated in one shut-down and one startup events are calculated according to Eq. (7), and summarized in Table 1.

Fig. 30 shows the yearly contributions of each wind speed to the fatigue damages in the bolts. The values summarized in the chart indicate that the low probabilities of higher wind speeds compensate for the larger stress ranges.

Fatigue life of each bolt can be estimated by reciprocal of the total damage index accumulated in 1 year. Using the damage values summarized in Table 1, fatigue lives of the bolts can be estimated for any specific number of shutdowns and startups per year. Figs. 31 and 32 show the estimated fatigue lives.

## 6. Conclusions

A numerical procedure for estimating the fatigue lives of connection bolts of wind turbine towers is established. Uncertainties related to wind are taken into account by probability distributions of short-term average (mean) wind speed and turbulence intensity. Methods of adjusting the statistical parameters of the wind for a specific site based on

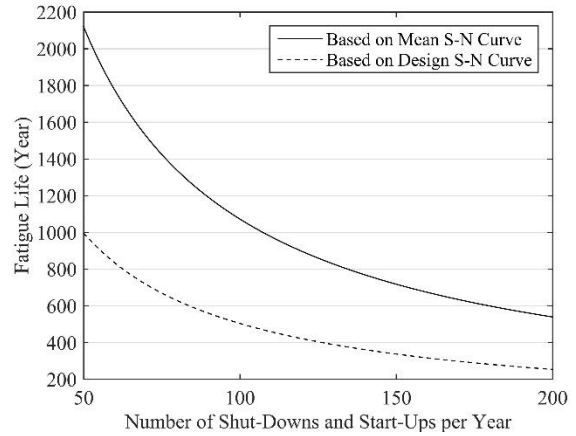


Fig. 31 Fatigue life estimation for the bolt at 233° Position

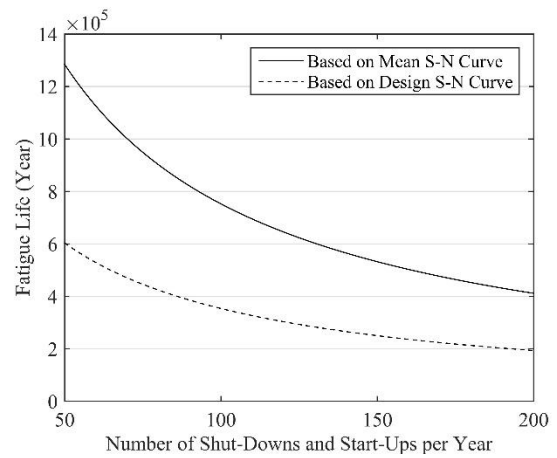


Fig. 32 Fatigue life estimation for the bolt at 110° Position

wind speed measurements are developed. Moreover, a method is developed that provides a possibility of representing the variability of wind parameters by a set of specific values for those parameters, derived from their probability distributions.

In finite element modeling of the bolted connection, interactions between the connected flanges, preloads in the bolts, and correct application of boundary conditions (calculated by aero-dynamic analyses) are among the factors that have considerable effects on accuracy of numerical results. The developed finite element model of the bolted connection achieves the required accuracy in a computationally efficient way, which is applicable in the industry. Measurements of strain in bolts show the validity of numerically obtained stress time-series, in terms of power density spectra and the resulting fatigue damage.

Positions of the bolts in the connection significantly affect the demands imposed on the bolts. It is clearly observed that the more distance each bolt has from the neutral axis of the major bending moment caused by wind, the more it is affected by the overturning moment in the connection, and thus it experiences more fatigue damage and has less fatigue life.

Fatigue lives of bolts in a wind turbine tower depend on many case-specific factors including the behavior of

electro-mechanical control systems of the turbine, operational strategy of the owner, quality of construction and quality of parts. This paper presents a method which is applicable for any specific wind turbine tower. Therefore, the fatigue damage estimations made in this paper are intended to demonstrate how different factors and states of operation contribute to the fatigue damage in the bolts, and how they can be taken into consideration in the fatigue analysis.

## Acknowledgments

Authors acknowledge the financial funding of TUBITAK with the grant number of 215M805 and they are also thankful to Assoc. Prof. Emre Otay and Mr. Soner Melih Kural for sharing the SCADA data.

## References

- ABAQUS (1998), "User's Manual, Hibbitt, Karlsson, and Sorensen, Inc., Providence, RI, U.S.A.
- Ahmed, A., Ahmad, S.P. and Reshi, J.A. (2013), "Bayesian analysis of Rayleigh distribution", *Int. J. Sci. Res. Publications*, **3**(10), 1-9.
- ASTM (American Society for Testing and Materials) (1997), "Standard practices for cycle counting in fatigue analysis", ASTM E1049-85 (Reapproved 2011), ASTM Int., West Conshohocken, U.S.A.
- Benedetti, M., Fontanari, V. and Battisti, L. (2013), "Structural health monitoring of wind towers: residual fatigue life estimation", *Smart. Mater. Struct.*, **22**(4), 045017. <https://doi.org/10.1088/0964-1726/22/4/045017>.
- Blachowski, B. and Gutkowski, W. (2016), "Effect of damaged circular flange-bolted connections on behaviour of tall towers, modelled by multilevel substructuring", *Eng. Struct.*, **111**, 93-103. <https://doi.org/10.1016/j.engstruct.2015.12.018>.
- Chou, J.S. and Tu, W.T. (2011), "Failure analysis and risk management of a collapsed large wind turbine tower", *Eng. Fail. Anal.*, **18**(1), 295-313. <https://doi.org/10.1016/j.engfailanal.2010.09.008>
- DNVGL (Det Norske Veritas Germanischer Lloyd) (2016a), "Fatigue design of offshore steel structures", Oslo, Norway.
- DNVGL (Det Norske Veritas Germanischer Lloyd) (2016b), "Support structures for wind turbines", Oslo, Norway.
- Do, T.Q., van de Lindt, J.W. and Mahmoud, H. (2014a), "Fatigue life fragilities and performance-based design of wind turbine tower base connections", *J. Struct. Eng.*, **141**(7), 04014183. [https://doi.org/10.1061/\(ASCE\)ST.1943-541X.0001150](https://doi.org/10.1061/(ASCE)ST.1943-541X.0001150).
- Do, T.Q., Mahmoud, H. and van de Lindt, J.W. (2014b), "Fatigue life of wind turbine tower bases throughout Colorado", *J. Perform. Constr. Fac.*, **29**(4), 04014109. [https://doi.org/10.1061/\(ASCE\)CF.1943-5509.0000612](https://doi.org/10.1061/(ASCE)CF.1943-5509.0000612).
- Elshaer, A., Bitsuamlak, G. and Abdallah, H. (2019), "Variation in wind load and flow of a low-rise building during progressive damage scenario", *Wind Struct.*, **28**(6), 389-404. <https://doi.org/10.12989/was.2019.28.6.389>.
- Eurocode (2005a), "Design of steel structures - Part 1-1: General rules and rules for buildings", European Committee for Standardization, Brussels, Belgium.
- Eurocode (2005b), "Design of steel structures - Part 1-9: Fatigue", European Committee for Standardization, Brussels, Belgium.
- GL (Germanischer Lloyd) (2010), "Guideline for the certification of wind turbines",
- Gol-Zaroudi, H. and Aly, A.M. (2017), "Open-jet boundary-layer processes for aerodynamic testing of low-rise buildings", *Wind Struct.*, **25**(3). <https://doi.org/10.12989/was.2017.25.3.233>
- Gunter, W.S., Schroeder, J.L., Weiss, C.C. and Bruning, E.C. (2017), "Surface measurements of the 5 June 2013 damaging thunderstorm wind event near Pep, Texas", *Wind Struct.*, **24**(2), 185-204. <https://doi.org/10.12989/was.2017.24.2.185>.
- Hanbay, S. (2019), "Vibration-based structural health monitoring of a wind turbine incorporating environmental and operational conditions", Master's Thesis, Bogazici University, Istanbul, Turkey.
- Heistermann, C., Husson, W. and Veljkovic, M. (2009), "Flange connection vs. friction connection in towers for wind turbines", *Proceedings of Nordic steel and construction conference, Stockholm, Sweden, September*.
- Hamdi, H. and Farah, K. (2018), "Beam finite element model of a vibrate wind blade in large elastic deformation.", *Wind Struct.*, **26**(1), 25-34. <https://doi.org/10.12989/was.2018.26.1.025>
- Huang, W. and Zhang, X. (2019), "Wind field simulation over complex terrain under different inflow wind directions", *Wind Struct.*, **28**(4), 239-253. <https://doi.org/10.12989/was.2019.28.4.239>
- IEC (International Electrotechnical Commission) (2005), "Wind turbines part 1: Design requirements." International Electrotechnical Commission.
- Ilhan, A., Bilgili, M. and Sahin, B. (2018), "Analysis of aerodynamic characteristics of 2 MW horizontal axis large wind turbine.", *Wind Struct.*, **27**(3), 187-197. <https://doi.org/10.12989/was.2018.27.3.187>
- Jonkman, J.M. and Buhl Jr, M.L. (2005), "FAST user's guide", National Renewable Energy Laboratory, Golden, CO, Technical Report No. NREL/EL-500-38230.
- Jonkman, B.J. and Klicher, L. (2012), "TurbSim user's guide: Version 1.06", National Renewable Energy Laboratory.
- Ke, S., Yu, W., Wang, T., Zhao, L. and Ge, Y. (2016), "Wind loads and load-effects of large scale wind turbine tower with different halt positions of blade", *Wind Struct.*, **23**(6), 559-575. <http://dx.doi.org/10.12989/was.2016.23.6.559>.
- Lu, C.L., Li, Q.S., Huang, S.H., Tuan, A.Y., Zhi, L.H. and Su, S. C. (2016), "Evaluation of wind loads and wind induced responses of a super-tall building by large eddy simulation", *Wind Struct.*, **23**(4), 313-350. <http://dx.doi.org/10.12989/was.2016.23.4.313>.
- Mao, W. and Zhou, Z. (2017), "Ground effects on wind-induced responses of a closed box girder", *Wind Struct.*, **25**(4), 397-413. <https://doi.org/10.12989/was.2017.25.4.397>
- Mirfazli, S.K., Giahi, M.H. and Dehkordi, A.J. (2019), "Numerical optimization of a vertical axis wind turbine: case study at TMU campus", *Wind Struct.*, **28**(3), 191-201. <https://doi.org/10.12989/was.2019.28.3.191>.
- Nowak, A.S. and Collins, K.R. (2000), "Reliability of Structures", McGraw Hill, U.S.A.
- Oechsner, M., Beyer, J., Simonsen, F., Schaumann, P. and Eichstädt, R. (2015), "Experimental and Analytical Assessment of the Fatigue Strength of Bolts with Large Dimensions under Consideration of Boundary Layer Effects.", *Proceedings of 2nd European Steel Technology and Application Days*, Düsseldorf, Germany.
- Pavlović, M., Heistermann, C., Veljković, M., Pak, D., Feldmann, M., Rebelo, C. and da Silva, L.S. (2015), "Friction connection vs. ring flange connection in steel towers for wind converters", *Eng. Struct.*, **98**, 151-162. <https://doi.org/10.1016/j.engstruct.2015.04.026>.
- Pedersen, N.L. and Pedersen, P. (2008a), "Stiffness analysis and improvement of bolt-plate contact assemblies", *Mech. Based Des. Struct.*, **36**(1), 47-66. <https://doi.org/10.1080/15397730701735749>.

- Pedersen, N.L. and Pedersen, P. (2008b), "On prestress stiffness analysis of bolt-plate contact assemblies", *Arch. Appl. Mech.*, **78**(2), 75-88. <https://doi.org/10.1007/s00419-007-0142-0>.
- Pollino, M.C. and Huckelbridge, A.A. (2012), "In-situ measurements of fatigue demands on a wind turbine support structure", *Proceedings of Energytech, IEEE*, Cleveland, U.S.A., May. <https://doi.org/10.1109/EnergyTech.2012.6304680>.
- Robinson, C., Paramasivam, E., Taylor, E., Morrison, A. and Sanderson, E. (2013), "Study and development of a methodology for the estimation of the risk and harm to persons from wind turbines", Health and Safety Executive, U.K.
- Schaumann, P. and Eichstädt, R. (2015), "Fatigue assessment of high-strength bolts with very large diameters in substructures for offshore wind turbines", *Proceedings of The Twenty-fifth International Ocean and Polar Engineering Conference, International Society of Offshore and Polar Engineers*, Kona, Hawaii, U.S.A, June.
- Seidel, M. and Schaumann, P. (2001), "Measuring fatigue loads of bolts in ring flange connections", *Proceedings of European conference, Wind Energy*, Copenhagen, Denmark.
- Shirani, M. and Härkegård, G. (2011a), "Fatigue life distribution and size effect in ductile cast iron for wind turbine components", *Eng. Fail. Anal.*, **18**(1), 12-24. <https://doi.org/10.1016/j.engfailanal.2010.07.001>.
- Shirani, M. and Härkegård, G. (2011b), "Large scale axial fatigue testing of ductile cast iron for heavy section wind turbine components", *Eng. Fail. Anal.*, **18**(6), 1496-1510. <https://doi.org/10.1016/j.engfailanal.2011.05.005>.
- SHK (Statens haverikommission) (2017), "Accident with a wind turbine in Lemnhult, Vetlanda municipality, Jönköping County, December 24, 2015", Report Number: RO 2017:01, Diary Number: O-08/15, Swedish Accident Investigation Authority, Stockholm, Sweden. <http://www.havkom.se/utredningar/vaegtrafik-oevrigt/olycka-med-vindkraftverk-i-lemnhult>
- Van-Long, H., Jean-Pierre, J. and Jean-François, D. (2013), "Behaviour of bolted flange joints in tubular structures under monotonic, repeated and fatigue loadings I: Experimental tests", *J. Constr. Steel Res.*, **85**, 1-11. <https://doi.org/10.1016/j.jcsr.2013.02.011>.
- Williams, J.G., Anley, R.E., Nash, D.H. and Gray, T.G.F. (2009), "Analysis of externally loaded bolted joints: Analytical, computational and experimental study", *Int. J. Pres. Ves. Pip.*, **86**(7), 420-427. <https://doi.org/10.1016/j.ijpvp.2009.01.006>.

## Appendix A: Estimation of long-term average of wind speed

Wind speeds are recorded by an ultrasonic device of the weather station at 60 m height from ground. However, for aerodynamic simulations of the wind turbine, wind speeds at the hub height (55 m) are needed. The Power-Law described by (Jonkman and Klicher 2012, Huang and Zhang 2019, Mirfazli *et al.* 2019) and given in Eq. (8) is used for correcting the wind speeds for hub height.

$$u_{\text{hub}} = u_{\text{measurement}} \left( \frac{h_{\text{hub}}}{h_{\text{measurement}}} \right)^m \quad (8)$$

where,  $h_{\text{measurement}} = 60\text{m}$  is the height of the measurement device,  $u_{\text{measurement}}$  is the wind speed measured by the device,  $h_{\text{hub}}$  is the height of the turbine hub,  $u_{\text{hub}}$  is the wind speed at hub height, and  $m$  is the exponent for the Power-Law, for which an average value of  $m = 0.2$  is assumed here according to Jonkman and Klicher (2012).

In order to estimate the long-term average of wind speed ( $V_{\text{ave}}$ ) based on the recorded wind speed measurements, a method suggested by Ahmed *et al.* (2013) is used. According to Ahmed *et al.* (2013), for a random variable  $x$  which has a Rayleigh distribution with the PDF given by Eq. (9), the parameter  $\eta$  of the distribution can be estimated by the value  $\hat{\eta}$  given by Eq. (10).

$$f_x(x) = \frac{x}{\eta^2} \exp\left(-\frac{x^2}{2\eta^2}\right) \quad (9)$$

$$\hat{\eta} = \frac{\Gamma\left(\frac{2n-1}{2}\right)}{\Gamma(n)} \sqrt{\frac{\sum_{i=1}^n x_i^2}{2}} \quad (10)$$

where,  $x_i$  are the  $n$  values of the sample of observations of the random variable  $x$ , and  $\Gamma$  is the gamma function. Therefore, for the PDF of  $V_a$  given by Eq. (2), the parameter  $V_{\text{ave}}$  is estimated by the value  $\hat{V}_{\text{ave}}$  given by Eq. (11):

$$\hat{V}_{\text{ave}} = \sqrt{\frac{\pi}{2}} \frac{\Gamma\left(\frac{2n-1}{2}\right)}{\Gamma(n)} \sqrt{\frac{\sum_{i=1}^n V_{ai}^2}{2}} \quad (11)$$

where  $V_{ai}$  are the  $n = 277$  values of the sample of observations of the random variable  $V_a$ .

## Appendix B: Estimation of mean and standard deviation of turbulence Intensity

In Fig. 33, the linear relationship (Eq. (3)) suggested for mean of  $\sigma_V$  by IEC (2005) is shown by a dotted line. The

scattered dots show  $\sigma_V$  vs  $V_a$  pairs of individual measurements by the weather station between 2015/04/01, 0:00 and 2015/04/02, 23:50. Measurements are converted to wind speed at hub height, using Eq. (8). It is clearly observed from Fig. 33 that the relationship suggested by IEC (2005) (Eq. (3)) overestimates the mean of  $\sigma_V$  for each value of  $V_a$ . Therefore, in this research  $\mu_{\sigma_V|V_a}$  (mean of  $\sigma_V$  for any specific value of  $V_a$ ) is calculated by a linear relationship shown in Fig. 33 by a solid line fitted to the measurements by a regression analysis.

According to Eq. (1), for every given value of  $V_a$ ,  $TI$  is equal to the log-normally distributed random variable

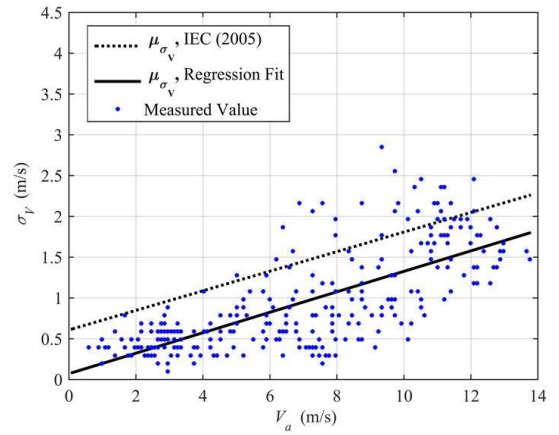


Fig. 33 Adjusting the linear relationship for mean of  $\sigma_V$

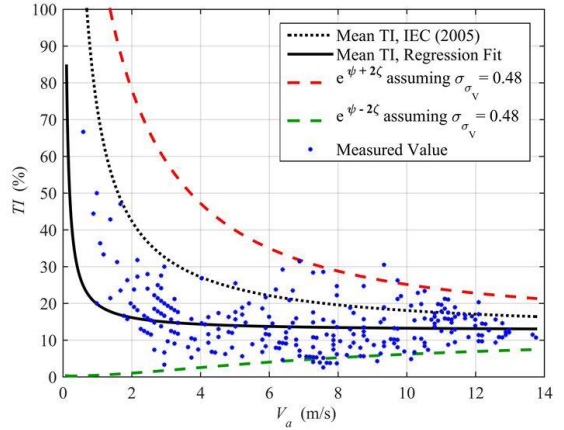


Fig. 34 Adjusting the standard deviation of  $\sigma_V$

$\sigma_V$  divided by a constant  $V_a$ . Therefore,  $TI$  is also log-normally distributed, and based on the rules governing the linear functions of random variables (Nowak and Collins, 2000) has mean and standard deviation values given by Eqs. (12) and (13).

$$\mu_{TI|V_a} = \frac{\mu_{\sigma_V|V_a}}{V_a} \quad (12)$$

$$\sigma_{TI|V_a} = \frac{\sigma_{\sigma_v|V_a}}{V_a} \quad (13)$$

Fig. 34 shows the variations of  $TI$  for different values of  $V_a$ . The dotted line represents the suggestion of IEC (2005) (According to Eqs. (3), (12)), the solid line is obtained by dividing the regression line of Fig. 33 by the  $V_a$  axis values, according to Eq. (12), and the scattered dots show the same individual measurements as shown in Fig. 33. Since  $TI$  has a lognormal probability distribution,  $\mathbf{Ln}(TI)$  has a normal probability distribution with the mean and standard deviation denoted by  $\psi$  and  $\zeta$  respectively. Therefore, 95.4% of  $\mathbf{Ln}(TI)$  values should be inside the interval  $\psi - 2\zeta \leq \mathbf{Ln}(TI) \leq \psi + 2\zeta$ . As a result, 95.4% of  $TI$  values should be inside the interval  $e^{\psi-2\zeta} \leq TI \leq e^{\psi+2\zeta}$ . The upper and lower limits of this interval are plotted as dashed envelope curves in Fig. 34. The right hand side of Eq. (4) suggested by IEC (2005) for  $\sigma_{\sigma_v}$  (standard deviation of  $\sigma_v$ ) is changed here to a value of  $\sigma_{\sigma_v} = 0.48$  in order to have 95.4% of measurements inside the two envelope curves. Based on the adjustments made above and using Eqs. (12) and (13), in this research, for any specific value of  $V_a$ , mean and standard deviation of  $TI$  are calculated using Eqs. (5) and (6).